JOURNAL OF NANO- AND ELECTRONIC PHYSICS
Vol. **17** No 4, 04009(7pp) (2025)

ЖУРНАЛ НАНО- ТА ЕЛЕКТРОННОЇ ФІЗИКИ
Том **17** № 4, 04009(7cc) (2025)

OPEN ACCESS

REGULAR ARTICLE

Improvement in the Gas Detection Capacity of ZnO-based Sensor: Impact of Static Potential

D.K. Chaudhary[1,2*], R. Shrestha[1], Y.R. Panthi[3,4], M. Slouf[3], L.P. Joshi[1], S.P. Shrestha[5†]

[1] *Department of Physics, Amrit Campus, Tribhuvan University, 44600 Kathmandu, Nepal*
[2] *Central Department of Physics, Tribhuvan University, 44618 Kathmandu, Nepal*
[3] *Institute of Macromolecular Chemistry, Czech Academy of Sciences, 162 06 Prague 6, Czech Republic*
[4] *Faculty of Mathematics and Physics, Charles University, 121 16 Prague, Czech Republic*
[5] *Department of Physics, Patan Multiple Campus, Tribhuvan University, Lalitpur, Nepal*

(Received 23 May 2025; revised manuscript received 20 August 2025; published online 29 August 2025)

The gas detection using metal oxide semiconductor (MOS) nanomaterials is rising. Among numerous MOS, ZnO is a feasible candidate for gas detection. ZnO-based gas sensor working at high operating temperatures is mostly reported. As the high-temperature operation reduces the long-term stability of the sensor, more research work has to be done to develop a room-temperature gas sensor. Because of low thermal energy at room temperature, the availability of electrons on the ZnO surface and the adsorption of oxygen molecules is low, which results in the low gas response. In this prospectus, this work reports a novel method of enhancing the gas sensing efficacy of MOS-based gas sensors at ambient temperature. In this work, the ZnO film was synthesized adopting the spray pyrolysis route and was characterized by X-ray diffraction (XRD), UV-Visible spectroscopy, and scanning electron microscopy (SEM). The static potential of 0-24 V was applied to the spray-coated nanostructured ZnO film to increase its oxygen adsorption capacity on its surface, and then its ammonia sensing ability was measured at ambient temperature. The gas sensing measurements showed the enhancement of gas response from 30.290 ± 0.042 at 0 V to 54.581 ± 0.062 at 24 V. It also showed quick response with a response/recovery time of 4/338 at 24 V. Thus, this report claims that the application of DC potential could be one of the useful alternative methods of achieving a MOS-based gas sensor working with a significant response.

Keywords: ZnO film, Spray pyrolysis, Gas sensing, Response, Static potential.

DOI: 10.21272/jnep.17(4).04009

PACS numbers: 77.55.hf, 81.15.Rs, 68.55. – a, 07.07 – Df

1. INTRODUCTION

Ammonia, ethanol and acetone are volatile and toxic chemicals that are used in common places. Ammonia is highly used in food processing, medical diagnosis, manufacturing nitrogenous fertilizers, industrial refrigerants, etc., [1, 2]. Acetone is used in pharmaceuticals for producing pills, liquid medicines, as an antiseptic and in the textile industry for decreasing wool and degumming silk [3]. Ethanol is mostly consumed for different applications such as food additives, antiseptics, fuel, antifreeze, industrial and commercial solvents, and antibacterial products [4]. In this regard, the global production of these gases is significantly increasing [2, 4, 5]. Direct exposure to these gases may cause severe health problems. For example, excessive exposure to ammonia may cause permanent blindness, throat and lung diseases and severe burns [6]. Acetone evaporates quickly at ambient temperature, and when exposed to humans, it can cause anesthesia and damage to the nervous system, liver, and kidneys [3]. Likewise, exposure to ethanol produces much damage, such as liver, ventricular and septal wall thickening [3, 6, 7]. Hence, early detection and monitoring of these toxic gases in all environments is necessary for health security. Several techniques have been employed to detect the leakages of these toxic gases, such as using conducting polymer [8], potentiometric electrodes [9], infrared devices, optical fibers [10], and metal oxide semiconductors (MOS) films. Among them, MOS-based devices have been found mostly preferred due to their cost-effectiveness and simplicity [11-13]. MOS used for gas detection are SnO_2, CuO, ZnO, Fe_2O_3, TiO_2, WO_3, V_2O_5 etc. [12, 14-18]. ZnO has emerged as one of the potential materials due to its easy tunable optical and electrical properties, high chemical and thermal stability, and nontoxic nature [2, 19].

Recently, the gas sensor based on ZnO nanostructures for various vapours/gases such as methanol, ethanol, acetone, ammonia, isopropanol, H_2, O_2, CO, CO_2, CH_4, H_2S etc. has been reported. Most of the reports showed the

* Correspondence e-mail: dinesh.chaudhary@ac.tu.edu.np
† shankarpds@yahoo.com

Cite this article as: D.K. Chaudhary et al., *J. Nano- Electron. Phys.* 17 No 4, 04009 (2025) https://doi.org/10.21272/jnep.17(4).04009

operating temperature greater than 300 °C [20-25]. As the high-temperature operation reduces the stability, a lot of work has been done to create gas sensors that respond well at room temperature or lower operating temperature, adopting various strategies including metal doping, nanocompositing and both. Only a few reports are available for the gas sensor working at room temperature [1, 26, 27]. Since few thermal electrons are available on the ZnO surface at room temperature or lower operating temperatures, few oxygen ions are adsorbed on the ZnO surface. These oxygen ions are thermally stable and difficult to extract from the ZnO surface. It results in low sensing performance at room temperature [25]. Hence, it is necessary to look at a strategy for developing a gas sensor working at room temperature with a higher response.

To increase the gas sensing abilities of ZnO, researchers adopted several strategies, including metal doping, functionalization, conducting polymer doping, UV-light activation, surface modification, etc., and succeeded in enhancing the gas sensing ability of ZnO [28-31]. Despite this; the scientists are attempting to use a novel approach to increase the gas detection capability even further. Keeping these factors in mind, this work presents a novel approach to improve the gas-sensing capability of ZnO. The ZnO film is subjected to a DC potential to enhance its oxygen adsorption ability. The gas sensing capacity was assessed at various DC applied potentials ranging from 0 to 24 V. Since our earlier paper [32] already reported on sensing characteristics such humidity effect, detection limit, selectivity, etc., this study solely focuses on the impact of DC applied potentials on the ammonia sensing ability of the spray-coated ZnO film and prospective gas detecting mechanism.

2. EXPERIMENTAL

2.1 Substrate Surface Cleaning

Cleaning the glass substrates before his film deposition is crucial for producing a uniform and sticky thin coating across the substrate's surface. The 76 mm × 26 mm × 2 mm commercially available glass substrates were first scrubbed with labeline detergent before being ultrasonically cleaned with acetone, deionized water, and then deionized water once again. After being cleaned, the glass substrates were dried in an oven set to 60°c for 30 minutes.

2.2 Preparation and Characterization of ZnO Thin Film

A 0.35M precursor solution was created by dissolving $Zn(CH_3COO)_2$:H_2O in deionized water using a magnetic stirrer at 60°C for 1 hr. It is then sprayed on the glass substrates at 380 °C using a nebulizer (CN-01W). The ZnO films were deposited due to evaporation, solute condensation, and pyrolytic decomposition of sprayed droplets of the precursor solutions. During film deposition, the parameters: glass nozzle to substrate distance (2 cm), nozzle diameter (0.2 cm), carrier gas flow rate (0.33 ml/min) and substrate temperature (380 ± 10°C), were kept fixed. The films were coated on the substrate up to 5 layers. The prepared film was characterized by scanning electron microscopy (SEM; MAIA3, TESCAN, Czech Republic), energy-dispersive analysis of X-rays (EDX; the EDX detector attached to the above-mentioned SEM microscope MAIA3) and X-ray diffraction (XRD; Explorer X-Ray diffractometer made by the GNR Analytical Instruments, Italy). The sample for SEM and EDX analysis was sealed with a carbon layer of thickness 4 nm to minimize charging and the EDX analysis was performed at low magnification and the accelerating voltage of 30 kV. Then the sample was sealed with a platinum layer of thickness 4 nm to further improve sample resistance to e-beam damage and charging, and its surface was observed at high magnification with the help of secondary electron imaging at an accelerating voltage of 3 kV. The XRD measurements were performed in theta-2theta geometry (2theta range 2-80°, angle step 0.01°, CuKα radiation with wavelength of 1.5406 Å.

2.3 Gas Sensing Setup

The schematic diagram of the gas sensor set-up is depicted in figure 1(a). It is made of a steel chamber. With three holes: one for the gas injection, another for connecting wires along with the thermocouple and the third one for the gas ejection. The gas seep was stopped by employing a cork and an iron O-ring. The zoom-in of the gas-sensing element (ZnO film on the glass substrate) with circuit diagram is depicted in Fig. 1(b). The FTO glass plate was held slightly above, parallel to the ZnO film. The ZnO film and FTO film was separated by 1.00 ± 0.07 mm with the help of an insulating support. Electrodes were made using silver paste and copper wire on the two ends of the ZnO film and the FTO film. The two electrodes from the ZnO film are joined to an LCR meter (IM3536, Hioki) to measure the resistance of the ZnO film in air and gas, respectively [Fig. 1 (b)]. The positive and negative terminals of the DC supply (0-30 V) were connected to the FTO glass plate and one of the electrodes of the ZnO film respectively to apply the static potential in the ZnO film. The gas response was measured by varying the applied static potential.

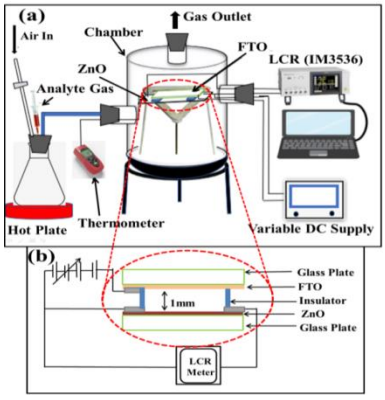

Fig. 1 – (a) Schematic of the gas sensor set up, (b) circuit diagram for gas sensing measurement at different applied static potentials

To get the required amount of ammonia vapour, a set volume of liquid ammonia was injected using a syringe into the airtight external conical flask. The flask was placed on the hot plate at a temperature of 120 ± 10°C and is joined to the chamber through a borosilicate glass tube [(Fig. 1 (a)]. The concentration of ammonia was calculated following the method explained in the previous report [28]. The ammonia vapour quickly dispersed from the conical flask to the ZnO film in the steel chamber. The analyte gas was ejected from the chamber by supplying air employing a nebulizer.

3. RESULTS AND DISCUSSION

3.1 Structural Characteristics

Fig. 2 depicts the XRD pattern of the ZnO film. A sharp diffraction peak at $2\theta = 34.42°$ was observed. This corresponded to the (002) interplanar of ZnO hexagonal structure (JCPDS card no. 36-1451). The other diffraction peaks disappeared in the background noise due to the fact that the ZnO layer was very thin. The d-spacing was estimated using Bragg's law: $2d \sin\theta = n\lambda$. The crystallite size (D) was estimated using Debye-Scherer's formula: $D = 0.9\lambda/\beta\cos\theta$ [34, 35]. Here, λ – wavelength of X-radiation, and β – full-width at half maxima of the diffraction peak. The values for d-spacing and D corresponding to the (002) plane were found to be 2.6023 Å and 37.97 nm, respectively.

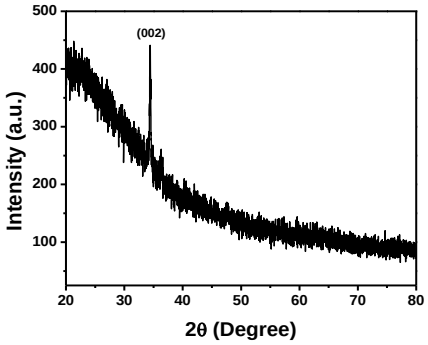

Fig. 2 – XRD pattern of the ZnO film

3.2 Optical Characteristics

The HR 4000 ocean optics spectrophotometer was used to measure the ZnO film's UV-Vis transmission spectrum in the wavelength range from 340 to 1000 nm. Figure 3(a) depicts the ZnO film's transmission spectrum. This shows that the average transmittance of the ZnO film exceeded 82% in the visible region. A sharp drop in transmittance was noted near the UV range. It is because of the fundamental absorption of light. The optical band gap (E_g) was evaluated from the Tauc plot: $(\alpha h\nu)^2 = A(h\nu - E_g)$ where α, A, and $h\nu$ are the absorption coefficient, energy constant, and photon energy, respectively [36]. Extrapolating the linear portion of the curve into the $h\nu$-axis yielded the value of E_g (band gap) of 3.297 ± 0.002 eV [Fig. 3(b)], which is in agreement with the published reports [37].

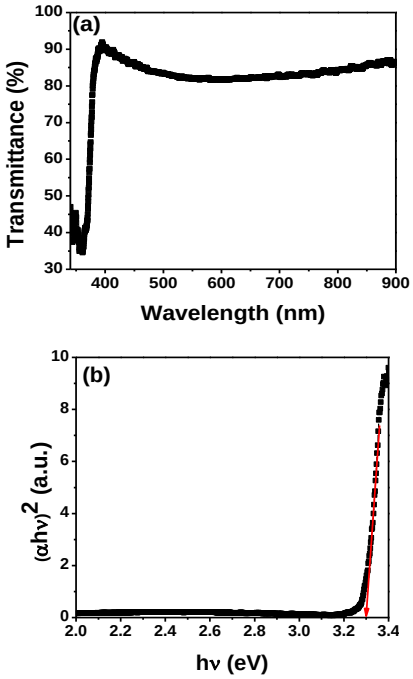

Fig. 3 – (a) Transmitance and (b) band gap of ZnO film

3.3 SEM and EDX Analysis

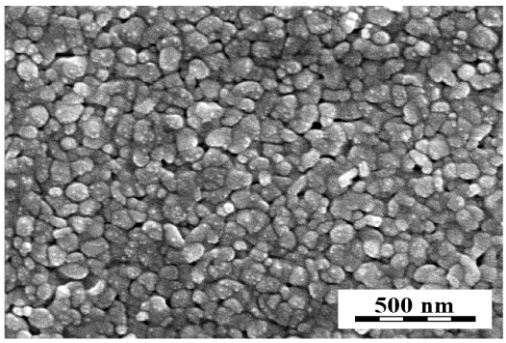

a

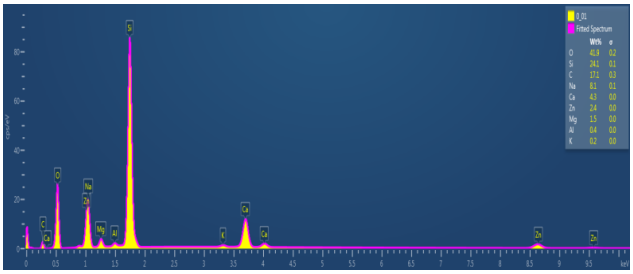

b

Fig. 4 – (a) SEM image and (b) EDX spectrum of ZnO film

The nature of the sensor surface plays a vital role in the gas-sensing task [38]. Fig. 4 (a) presents the SEM image of the ZnO film. It clearly shows the surface of spherical grains with a slightly porous structure. The

sample's elemental composition was confirmed by EDX analysis. EDX spectrum [Fig. 4(b)] showed sharp peaks corresponding to Zn and O, indicating the purity of the film. Other low-intensity peaks, corresponding to elements Si, C, Na, Ca, Mg, Al, and K, were also observed. The presence of these elements was due to the elements in the supporting glass substrate.

3.4 Sensing Characteristics

The gas sensing characteristics were examined by assessing the ZnO film's resistance in the air as well as in exposure to 400 ppm ammonia vapour at various applied static potentials. Fig. 5(a-e) shows the variation of ZnO film's resistance for 4 cycles of gas injection and ejection at different applied static potentials (0-24 V). A sharp reduction in the ZnO film's resistance resulted from the exposure to ammonia vapour, and then acquired stable minimum saturation values. The observed stable values of the ZnO film's resistances in the air (R_a) and in ammonia vapour (R_g) at different static potentials are presented in table 1. The resistance was decreased to almost the same lower values at all applied electrode potentials in 4 cycles, indicating good repeatability. But the base resistance of the film was increased with the applied potentials [Fig. 5(f)]. Therefore, the application of potentials resulted in a greater change in the ZnO film's resistance.

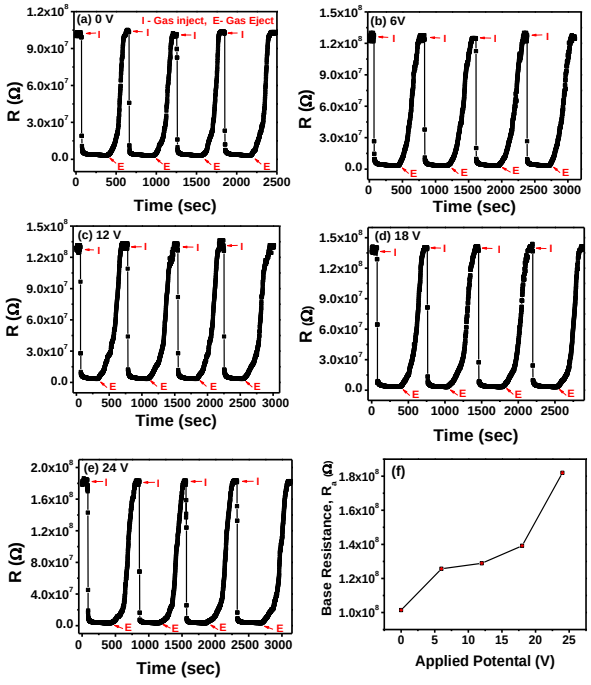

Fig. 5 – (a-e) ZnO film's resistance variation with time at 400 ppm NH3 exposure for 4 cycles, and (f) base resistance at applied potentials of 0-24 V

The gas response (R) was determined using the formula: $R = R_a/R_g$, where R_a and R_g represent the ZnO film's resistance in the air and gas, respectively [39]. The calculated value of gas response is presented in Table 1.

Table 1 – Base resistance (in air) and stable resistance in ammonia vapor and gas response at different potential

Applied Potential (V)	Base Resistance (in air) R_a, × 10^5 Ω	Stable Resistance in NH_3 R_g,× 10^3 Ω	Gas response (R_a/R_g)
0	1014.111 ± 1.567	3342.611 ± 3.708	30.292 ± 0.972
6	1256.511 ± 2.859	3462.071 ± 1.383	36.324 ± 1.150
12	1290.091 ± 2.486	3286.512 ± 3.699	38.893 ± 1.121
18	1391.372 ± 1.661	3291.921 ± 3.353	42.662 ± 0.672
24	1829.392 ± 2.093	3288.932 ± 1.992	54.581 ± 1.255

Fig. 6 shows the gas response at different applied potentials. The gas response was increased with an increase in the applied potentials. The enhancement in the gas response was due to the large change in the ZnO film's resistance after ammonia exposure in the presence of applied potentials.

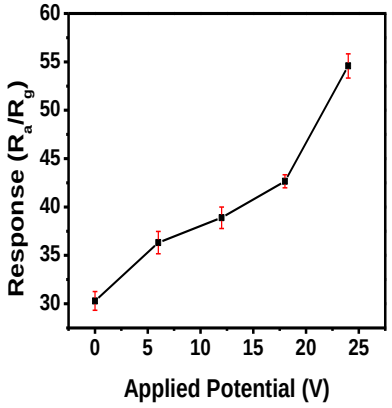

Fig. 6 – Gas response Vs applied potential

Fig. 7(a-e) represents the plot for variation of the ZnO film's resistance with time after injection/ejection of the NH_3 vapour for response/recovery time calculations.

The response/recovery time is the time needed to change the sensor signal (say, resistance) by 90% after injection/ejection of gas. The calculated response/recovery time at different potentials is depicted in Fig. 7(f). ZnO film showed a fast response with the response time of 4-5 sec at all potentials and a delayed recovery with recovery times of 186, 271, 337, 344 and 338 sec at potentials of 0, 6, 12, 18 and 24 V, respectively.

3.5 Sensing Mechanism

In Fig. 5(a)-(e), the ZnO film's resistance dropped precipitously before reaching the saturation value on exposure to the ammonia vapour. The ZnO film's resistance again increased and achieved the initial value after the ejection of ammonia vapor. In Fig. 5(f), the base

resistance of the film was increased on the application of potential. It can be illustrated using the classical model presented in Fig. 8(a-c).

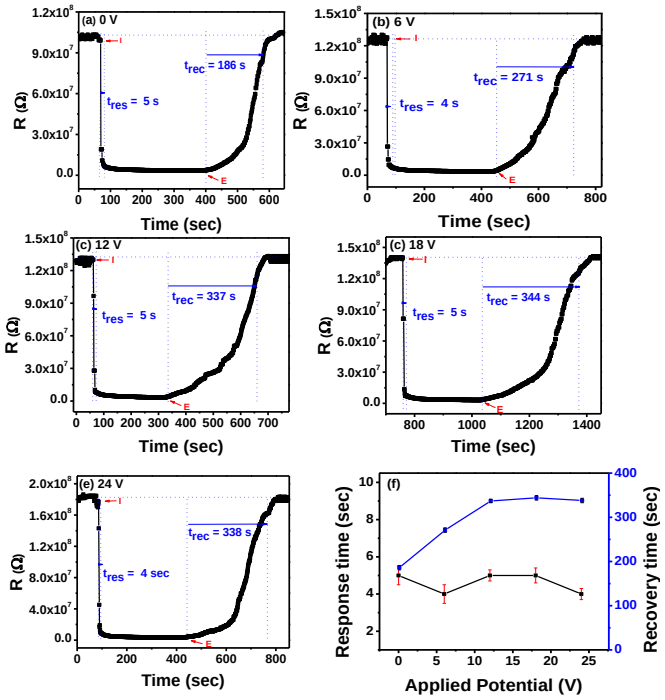

Fig. 7 – (a-e) Calculation of response/recovery times and (f) plot of response/recovery times at different potentials (0-24 V)

Fig. 8(a) depicts the adsorption of oxygen molecules onto the film's surface in the absence of applied potential in an air environment. The oxygen molecules extract the electrons from the conduction band and change into O_2^- ions. As a result, the depletion region as well as the potential barrier height increases. It increases the ZnO film's resistance up to the stable value. This resistance was chosen as the base resistance under the study and is denoted as R_a. When the potential is applied to the FTO surface, the positively charged FTO surface attracts the electrons from ZnO's conduction band, and additional O_2^- ions are adsorbed onto the ZnO surface by taking electrons from its conduction band. As a result, the depletion layer widened more, thereby increasing the potential barrier height and the film's resistance. Figure 8(b) illustrates this phenomenon. This explains why the applied potential raised the film's base resistance. When NH_3 vapor is exposed to ZnO films surface, NH_3 molecules interact with O_2^- ions, releasing electrons back to film's surface. This lowers the depletion layers and height of the potential barrier and hence the film's resistance, resulting in a steady value of resistance. This is illustrated in Figure 8(c). This explains why the film's resistance dropped as it was exposed to gas.

In Figure 6, the response increases with increasing applied potential. It is because the application of positive potential on the FTO surface increases O_2^- ions adsorption onto the ZnO surface and hence increases the value of base resistance, Ra. When the NH_3 vapour is exposed to the ZnO in the presence of the field, the NH_3 molecules interact with additional oxygen ions and an additional electron is liberated. It results in an additional change in the ZnO film resistance when the potential is applied, and a high response results. This phenomenon is illustrated in Fig. 8(c).

In Fig. 7(a-e), the ZnO exhibited fast response with a response time of 4-5 sec (nearly the same value) at all applied potentials. It is because the rate of interaction of NH3 molecules with adsorbed O_2^- ions determines the response time. The higher the reaction rate, the faster the release of electrons by O_2^- ions and the faster the response. Also, the interaction rate of the NH_3 molecules with the O_2^- ions was independent of the applied potential. Therefore, response time is nearly the same in all applied potentials. The faster the response. Also, the interaction rate of the NH_3 molecules with the O_2^- ions was independent of an applied potential. Therefore, response time is nearly the same in all applied potentials.

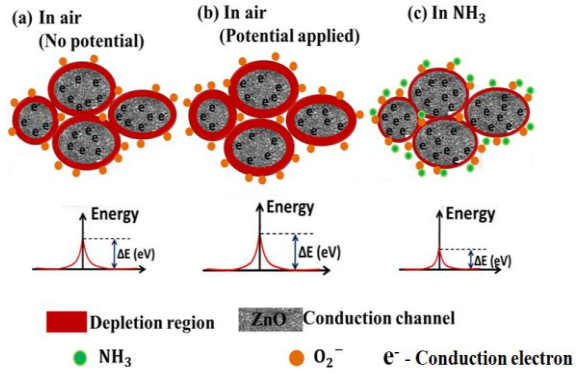

Fig. 8 – Sensing mechanism of the ZnO sensor: depletion region and barrier height of ZnO when (a) no potential, and (b) potential is applied in air, and (c) in NH_3 vapour environments

4. CONCLUSION

In summary, the ZnO film was synthesized using the spray pyrolysis route and characterized both optically and structurally. Its gas-sensing ability at room temperature was investigated by applying various static potentials (0-24 V) during exposure to 400 ppm ammonia. At increased potential, the gas response was enhanced. By increasing the applied potential from 0 to 24 V, the response value nearly doubled, rising from 30.292 ± 0.042 to 54.581 ± 0.062. The ZnO showed a fast response with a response time of 4-5 seconds at all applied potentials and slow recovery at the higher applied potentials. The result obtained in this work will be useful in constructing an efficient room-temperature gas sensor.

ACKNOWLEDGEMENTS

The author would like to thank the International Science Program, Uppsala University, Sweden, through the NEP-01 grant for the support on the instrumentation, and consumables. The author would also like to thank Milos Steinhart for the XRD experiment.

REFERENCES

1. G.K. Mani, J.B.B. Rayappan, *Mater. Sci. Eng. B.* **191**, 41 (2015).
2. V.B. Raj, A.T. Nimal, Y. Parmar, M.U. Sharma, K. Sreenivas, V. Gupta, *Sens. Actuators B Chem.* **147**, 517 (2010).
3. P. Song, D. Han, H. Zhang, J. Li, Z. Yang, Q. Wang, *Sensor. Actuat. B: Chem.* **196**, 434 (2014)
4. K. Roopa-Kishore, D. Balamurugan, B.G. Jeyaprakash, *J. Mater. Sci. Mater. Electron.* **32**, 1204 (2021).
5. N. Sarkar, S.K. Ghosh, S. Bannerjee, K. Aikat, *Renew. Energy.* **37**, 19 (2012).
6. G.K. Mani, J.B.B. Rayappan, *Sensor. Actuat. B: Chem.* **183**, 459 (2013).
7. A.J. Kulandaisamy, J.R. Reddy, P. Srinivasan, K.J. Babu, G.K. Mani, P. Shankar, J.B.B. Rayappan, *J. Alloy. Compd.* **688**, 422 (2016).
8. Z. Yang, Y. Huang, G. Chen, Z. Guo, S. Cheng, S. Huang, *Sensor. Actuat. B: Chem.* **140**, 549 (2009).
9. Y.C. Wong, B.C. Ang, A.S.M.A. Haseeb, A.A. Baharuddin, Y.H. Wong, *J. Electrochem. Soc.* **167**, 037503 (2020).
10. C. Wang, B. Yang, H. Liu, F. Xia, J. Xiao, *Sensor. Actuat. B: Chem.* **316**, 128140 (2020).
11. C. Elosua, I. Matias, C. Bariain, F. Arregui, *Sensors* **6**, 1440 (2006).
12. S.M. Chou, L.G. Teoh, W.H. Lai, Y.H. Su, M.H. Hon, *Sensors* **6** No 10, 1420 (2006).
13. S. Das, V. Jayaraman, *Prog. Mater. Sci.* **66**, 112 (2014).
14. Z. Li, Z. Yao, A.A. Haidry, T. Plecenik, L. Xie, L. Sun, Q. Fatima, *Int. J. Hydrog. Energy.* **43**, 21114 (2018).
15. S. Büyükköse, *Mater. Sci. Semicond. Process.* **110**, 104969 (2020).
16. K.S. Weißenrieder, J. Müller, *Thin Solid Film* **300** No 1, 30 (1997).
17. B. Karunagaran, P. Uthirakumar, S.J. Chung, S. Velumani, E-K. Suh, *Mater. Charact.* **58**, 680 (2007).
18. S. Steinhauer, E. Brunet, T. Maier, G.C. Mutinati, A. Köck, O. Freudenberg, C. Gspan, W. Grogger, A. Neuhold. R. Resel, *Sensor. Actuat. B: Chem.* **187**, 50 (2013).
19. H.M. Yang, S.Y. Ma, G.J. Yang, W.X. Jin, T.T. Wang, X.H. Jiang, W.Q. Li, *Mater. Lett.* **169**, 73 (2016).
20. L.P. Joshi, B.V. Khatri, S. Gyawali, S. Gajurel, D.K. Chaudhary, *J. Phys. Sci.* **32**, 15 (2021).
21. F. Paraguay, D.M. Miki-Yoshida, J. Morales, J. Solis, W. Estrada, *Thin Solid Films* **373**, 137 (2000).
22. V.T. Salunke, P.B. Buchade, A.D. Shaligram, R.Y. Borse, *IOP Conf. Ser. Mater. Sci. Eng.* **1263**, 012027 (2022).
23. J. Saydi, M. Karimi, M. Mazhdi, J. Seidi, F. Mazhdi, *J. Mater. Eng. Perform.* **23**, 3489 (2014).
24. E. Wongrat, N. Chanlek, C. Chueaiarrom, W. Thupthimchun, B. Samransuksamer, S. Choopun, *Ceram. Int.* **43**, S557 (2017).
25. X.L. Xu, Y. Chen, S.Y. Ma, W.Q. Li, Y.Z. Mao, *Sensor. Actuat. B: Chem.* **213**, 222 (2015).
26. L. Zhu, Y. Li, W. Zeng, *Ceram. Int.* **43**, 14873 (2017).
27. K. Lokesh, G. Kavitha, E. Manikandan, G.K. Mani, K. Kaviyarasu, J.B.B. Rayappan, R. Ladchumananandasivam, J. Sundeep Aanand, M. Jayachandran, M. Maaza, *IEEE Sens. J.* **16**, 2477 (2016).
28. M. Poloju, N. Jayababu, M.V. Ramana Reddy, *Mater. Sci. Eng. B.* **227**, 61 (2018).
29. D.K. Chaudhary, S.K. Joshi, S. Thapa, Y. Yue, P. Zhu, *J. Nano- Electron. Phys.* **16** No 2, 02011 (2024).
30. P. Rai, S.H. Jeon, C.H. Lee, J.H. Lee, Y.T. Yu, *RSC Adv.* **4** No 45, 23604 (2014).
31. J. Wuloh, E.S. Agorku, N.O. Boadi, *J. Sens.* **2023** No 1, 747986 (2023).
32. J. Gong, Y. Li, X. Cai, Z. Hu, Y. Deng, *J. Phys. Chem. C* **114** No 2, 1293 (2010).
33. D.K. Chaudhary, Y.S. Maharjan, S. Shrestha, S. Maharjan, S.P. Shrestha, L.P. Joshi, *J. Phys. Sci.* **33** No 1, 97 (2022).
34. T.R. Acharya, P. Lamichhane, R. Wahab, D.K. Chaudhary, B. Shrestha, L.P. Joshi, N.K. Kaushik, E.H. Choi, *Molecules* **26**, 7685 (2021).
35. N.G. Pramod, S.N. Pandey, *Ceram. Int.* **40**, 3461 (2014).
36. T. Srinivasulu, K. Saritha, K.T.R. Reddy, *Mod. Electron. Mater.* **3**, 76 (2017).
37. A.P. Rambu, V. Nica, M. Dobromir, *Superlattice. Microst.* **59**, 87 (2013).
38. F. Shao, J.D. Fan, F. Hernández-Ramírez, C. Fàbrega, T. Andreu, A. Cabot, J.D. Prades, N. López, F. Udrea, A. De Luca, S.J. Ali, J.R. Morante, *Sensor. Actuat. B: Chem.* **226**, 110 (2016).
39. A. Yu, J. Qian, H. Pan, Y. Cui, M. Xu, L. Tu, Q. Chai, X. Zhou, *Sensor. Actuat. B: Chem.* **158**, 9 (2011).
40. S. Bhatia, N. Verma, R.K. Bedi, *Res. Phys.* **7**, 801 (2017).

Покращення здатності датчика на основі ZnO до виявлення газу: вплив статичного потенціалу

D.K. Chaudhary[1,2], R. Shrestha[1], Y.R. Panthi[3,4], M. Slouf[3], L.P. Joshi[1], S.P. Shrestha[5]

[1] *Department of Physics, Amrit Campus, Tribhuvan University, 44600 Kathmandu, Nepal*
[2] *Central Department of Physics, Tribhuvan University, 44618 Kathmandu, Nepal*
[3] *Institute of Macromolecular Chemistry, Czech Academy of Sciences, 162 06 Prague 6, Czech Republic*
[4] *Faculty of Mathematics and Physics, Charles University, 121 16 Prague, Czech Republic*
[5] *Department of Physics, Patan Multiple Campus, Tribhuvan University, Lalitpur, Nepal*

Виявлення газу за допомогою наноматеріалів на основі металоксид-напівпровідників (МОП) набуває все більшої популярності. Серед численних МОП-транзисторів ZnO є можливим кандидатом для виявлення газу. Найчастіше повідомляється про газовий сенсор на основі ZnO, що працює за високих робочих температур. Оскільки робота за високих температур знижує довготривалу стабільність сенсора, необхідно провести більше досліджень для розробки газового сенсора для кімнатної температури. Через низьку теплову енергію за кімнатної температури, доступність електронів на поверхні ZnO та адсорбція молекул кисню є низькими, що призводить до низької реакції на газ. У цьому проспекті повідомляється про новий метод підвищення ефективності газового сприйняття на основі МОП-транзисторів за кімнатної температури.

У цій роботі плівку ZnO було синтезовано методом розпилювального піролізу та охарактеризовано за допомогою рентгенівської дифракції (XRD), УФ-видимої спектроскопії та скануючої електронної мікроскопії (CEM). Статичний потенціал 0-24 В було прикладено до нанесеної на наноструктуровану плівку ZnO, щоб збільшити її здатність до адсорбції кисню на її поверхні, а потім її здатність до сприйняття аміаку була виміряна за кімнатної температури. Вимірювання газового зондування показали покращення газової реакції з 30,290 ± 0,042 при 0 В до 54,581 ± 0,062 при 24 В. Також було продемонстровано швидку реакцію з часом реакції/відновлення 4/338 при 24 В. Таким чином, у цьому звіті стверджується, що застосування постійного потенціалу може бути одним із корисних альтернативних методів отримання газового сенсора на основі МОН, який працює зі значною реакцією.

Ключові слова: Плівка ZnO, Розпилювальний піроліз, Газові зонди, Відгук, Статичний потенціал.